Supplementary material to the manuscript "Shifting water scarcities: Irrigation alleviates agricultural green water deficits while increasing blue water scarcity"

Heindriken Dahlmann[1,2,3], Lauren S. Andersen[3], Sibyll Schaphoff[3], Fabian Stenzel[3,4], Johanna Braun[3], Christoph Müller[3] and Dieter Gerten[1,2,3]

[1]Integrative Research Institute on Transformations of Human-Environment Systems, Humboldt-Universität zu Berlin, Berlin, Germany
[2]Department of Geography, Humboldt-Universität zu Berlin, Berlin, Germany
[3]Potsdam Institute for Climate Impact Research (PIK), Member of the Leibniz Association, P.O. Box 60 12 03, D-14412 Potsdam, Germany
[4]Stockholm Resilience Centre, Stockholm University, Stockholm, Sweden

1 LPJmL simulations and data validations

Input data

Table S1: Main input data for LPJmL simulations.

Input	Description	Time period	Data source
Temperature	Daily mean near-surface air temperature	1901-2019	GSWP 5WE5 dataset (Lange et al., 2021)
Precipitation	Daily mean precipitation rate	1901-2019	
Longwave radiation	Daily net longwave radiation	1901-2019	
Shortwave radiation	Daily surface downwelling shortwave radiation	1901-2019	
Land use	Distribution of crop functional types and their respective rainfed and irrigated shares per grid cell	1500-2017	LandInG 1.0 (Ostberg et al., 2023)
Fertilizer	Crop-specific fertilizer rates	1860-2017	
Soil	Different types of soil texture	-	

Input	Description	Time period	Data source
HIL water use	Water use for domestic, industrial and livestock sector	1900-2000	Flörke et al., 2013

15

Model runs

Figure S1 provides a schematic representation of the LPJmL model runs. For this study, we ran a 3,500-year spin-up in order to bring the PFT and CFT distribution and carbon pools into equilibrium. Starting from 1901, we ran a limited irrigation run (ILIM), distinguishing between rainfed and irrigated agriculture. Irrigation in this run depends on water availability in rivers, 20 reservoirs and upstream neighboring cells from which irrigation water can also be withdrawn. For the analyses of this paper, we ran a second irrigation scenario which neglects irrigation and considers all agriculture to be rainfed (INO), this run started from the year 1900. For better comparability of irrigated CFTs in INO and ILIM, we modified the growing seasons of the irrigated CFTs in INO so that they match the original season lengths used in ILIM, avoiding any alignment with the rainfed growing season. We also implemented a groundwater buffer to represent subsurface water storage, which releases water at a 25 fixed rate of 0.01 per day relative to the current buffer volume. This adjustment is intended to simulate a simplified groundwater discharge process.

Figure S1: Schematic representation of the LPJmL model runs.

Data validation

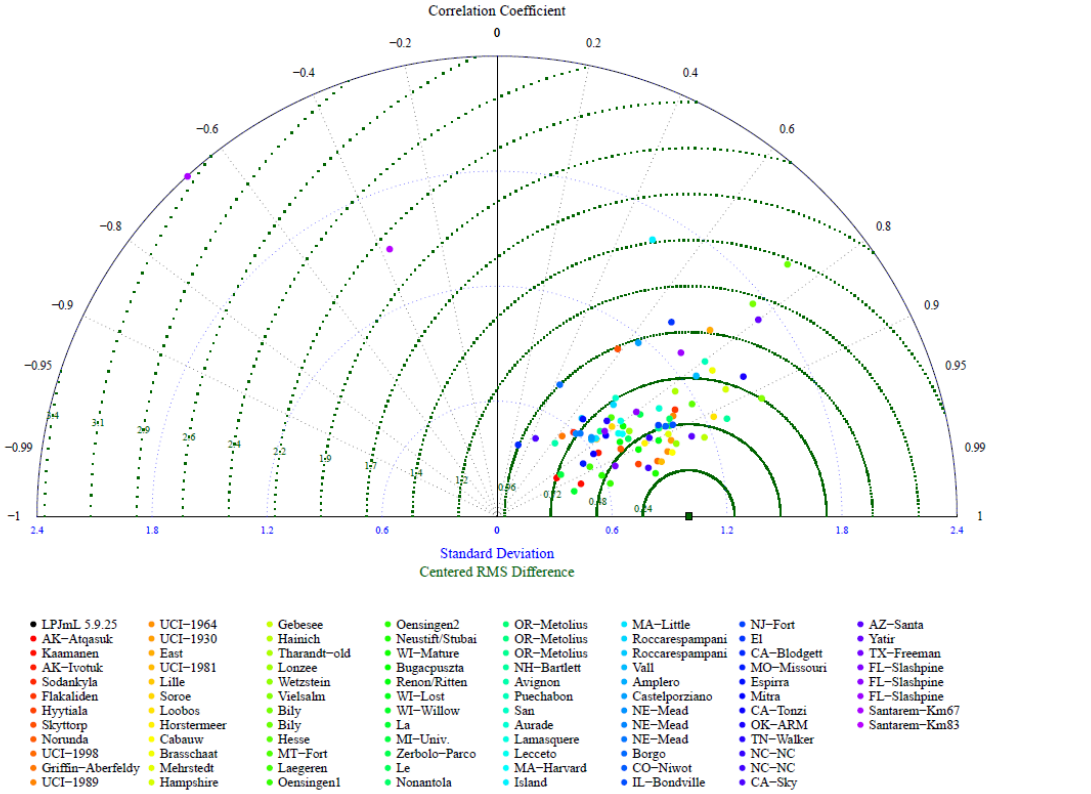

Figure S2: Validation of LPJmL 5.9.25 evaporation rates with evaporation rates measured at eddy flux towers: ORNL DAAC (2011). Available online at FLUXNET (http://fluxnet.fluxdata.org/data/la-thuile-dataset/). Site locations are ordered from north to south.

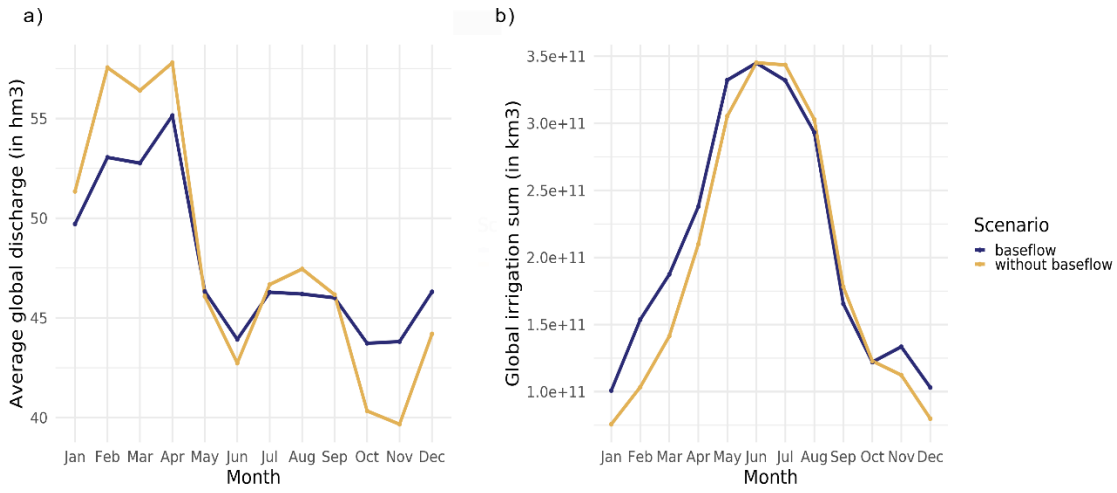

Figure S3: Comparison of a) the average global discharge and b) the global irrigation sum with and without the implemented baseflow.

2 GWS data comparison

For a comparison with the results of He and Rosa (2023), we adjusted our baseline to theirs (1996-2005) and compared the results of both green water stresses. The results show that with our GWS indicator, more severe GWS occurs in Africa and South America, but less in the USA and Europa. The limited GWS observed in the USA and Europe in our study is primarily due to the low atmospheric demand of crops grown during autumn and winter. In these regions, only a few CFTs are cultivated, mainly temperate cereals, tropical cereals, temperate roots, and oil crops such as sunflower, soybean, and rapeseed. For instance, temperate cereals experience GWS from May to August but not for the rest of the year if they are growing (see C9). Similarly, winter rapeseed, predominantly grown in Europe, does not face GWS between September and March. These seasonal patterns significantly influence the average GWS levels. The high GWS patterns He and Rosa (2023) found in the USA are only visible in the summer months in our analysis.

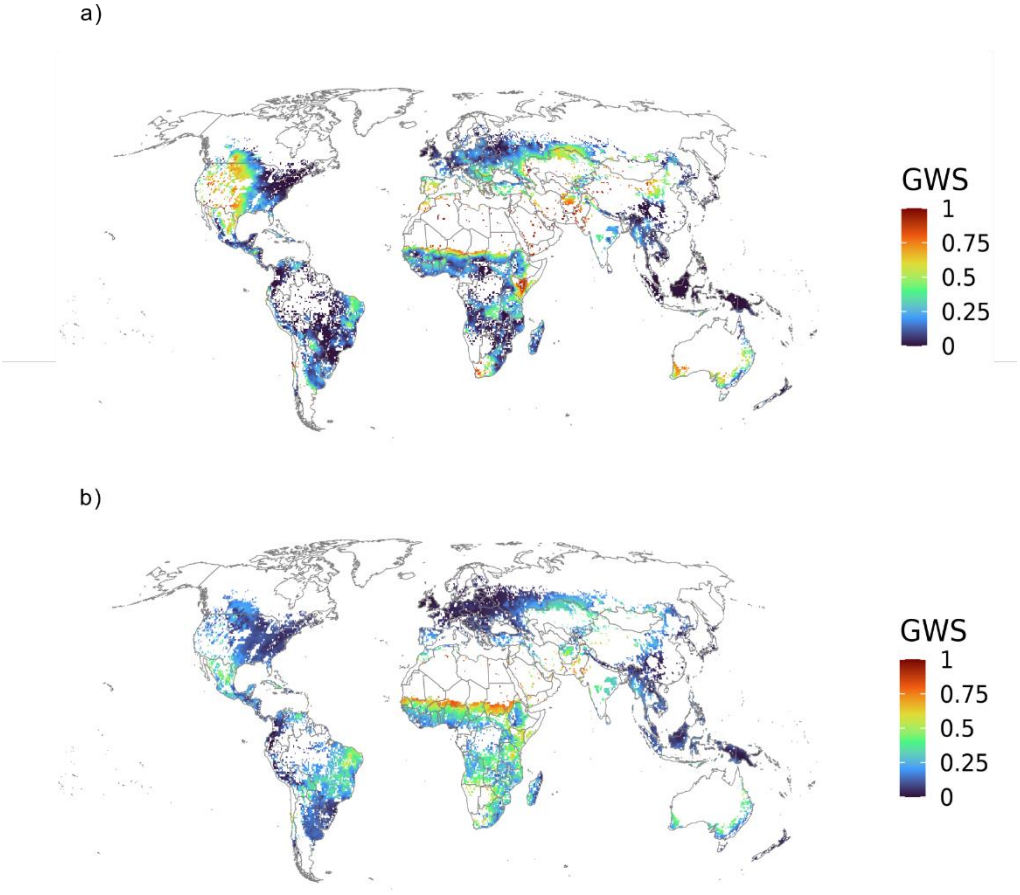

Figure S4: Comparison of GWS in this study to results of He and Rosa (2023): a) average GWS for time period 1996-2005 in He and Rosa (2023), b) average GWS of this study computed for time period 1996-2005 and cropped to spatial extent of He and Rosa (2023).

We further compared our results with the often used actual to potential evapotranspiration (AET/PET) ratio. The plant-specific GWS indicator developed in this study differs from the AET/PET ratio, as the latter reflects broader energy levels. Moreover, the AET/PET ratio accounts for total vegetation across all months within a grid cell, rather than focusing on crop-specific growing seasons. Nonetheless, regions with a high GWS indicator in our analysis tend to coincide with areas where the AET/PET ratio indicates drier conditions.

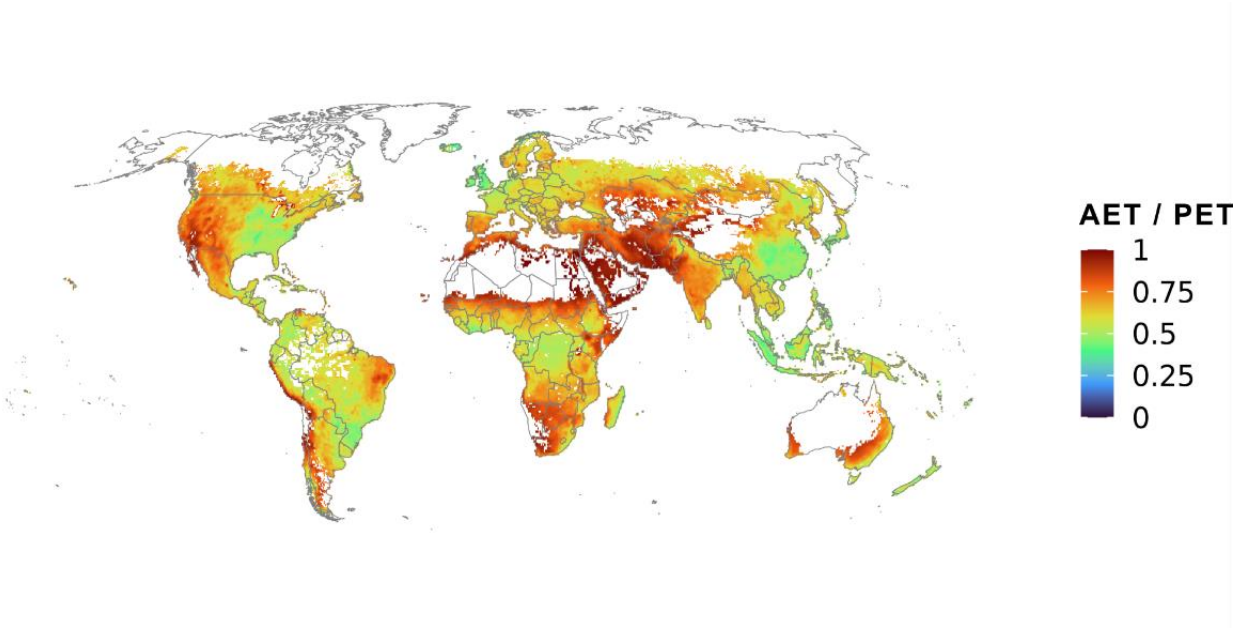

Figure S5: Actual evapotranspiration divided by potential evapotranspiration index (AET/PET) as average for the time period 2015-2019.

3 Supplementary results

Green water stress

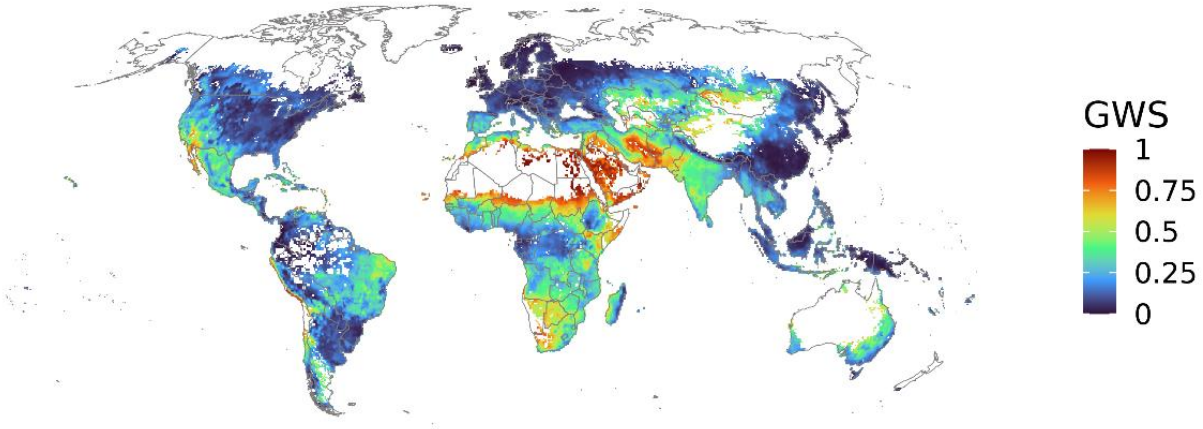

Figure S6: Average green water stress in ILIM for the time period 2015-2019 as yearly average over all CFTs and months.

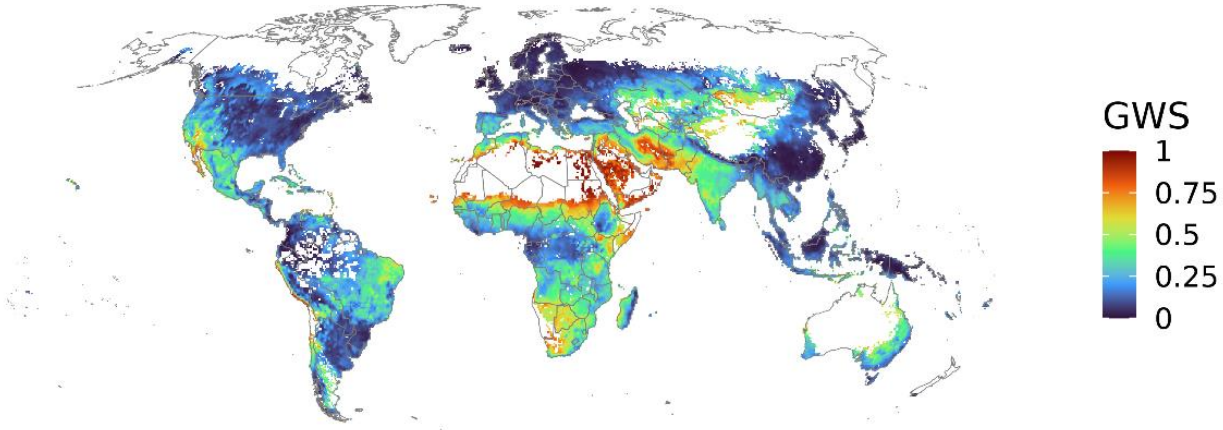

Figure S7: Average green water stress for rainfed CFTs in ILIM for the time period 2015-2019 as yearly average over all CFTs and months.

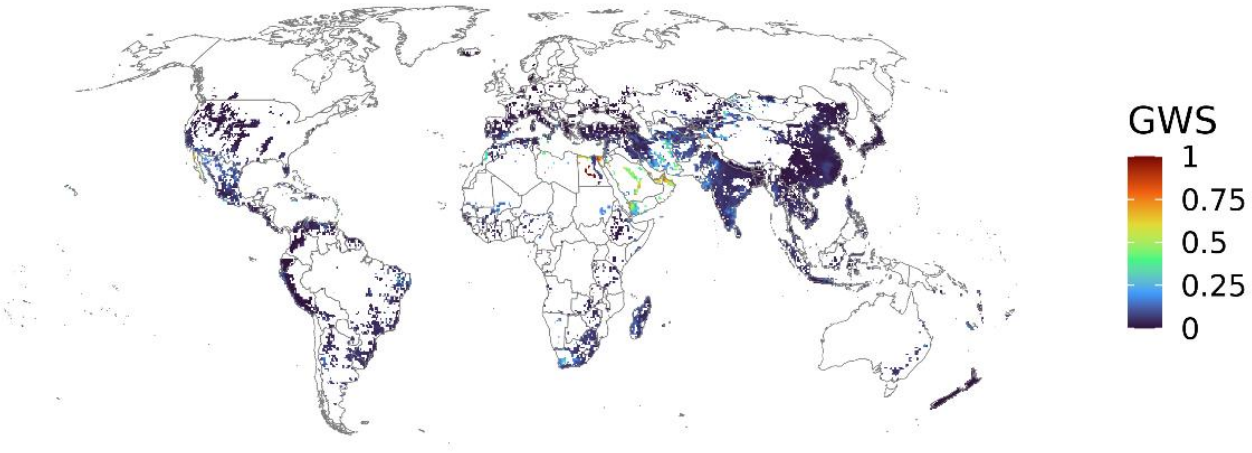

Figure S8: Average green water stress for irrigated CFTs in ILIM for the time period 2015-2019 as yearly average over all CFTs and months.

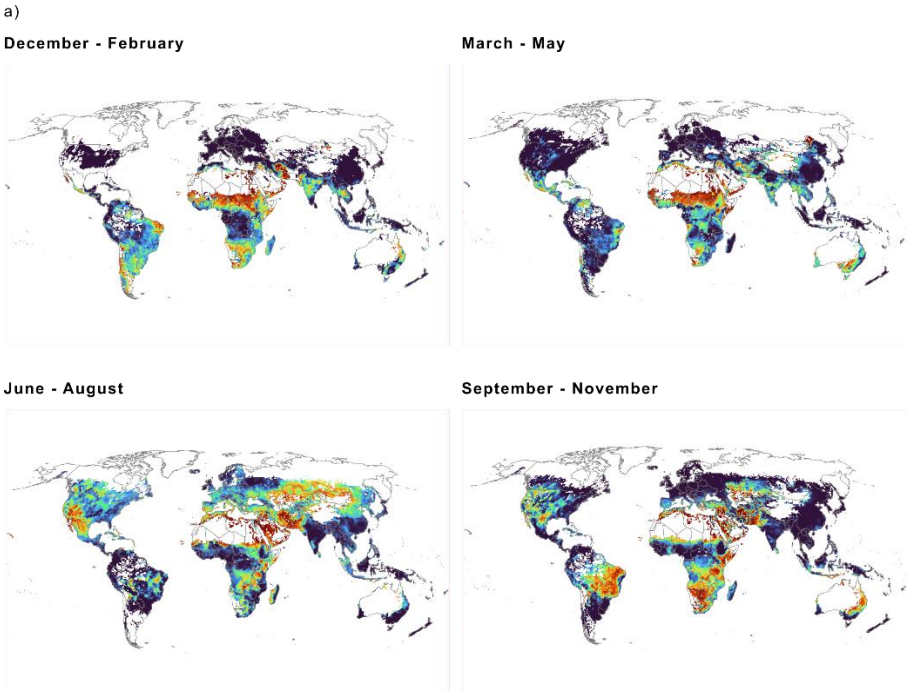

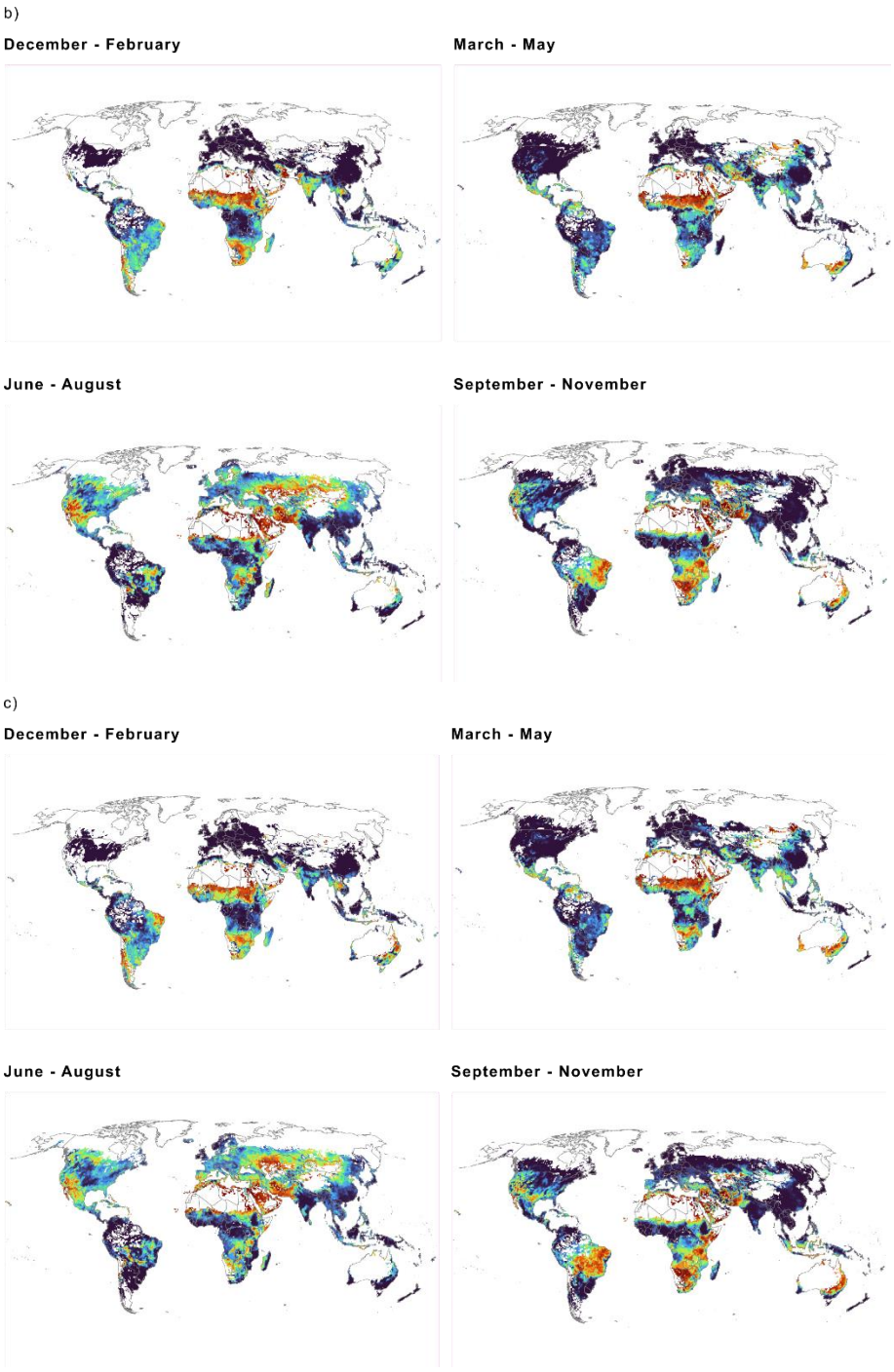

Figure S9: Comparison of GWS in different years. GWS on a seasonal scale, averaged over all CFTs in ILIM for the years a) 2017, b) 2018 and c) 2019.

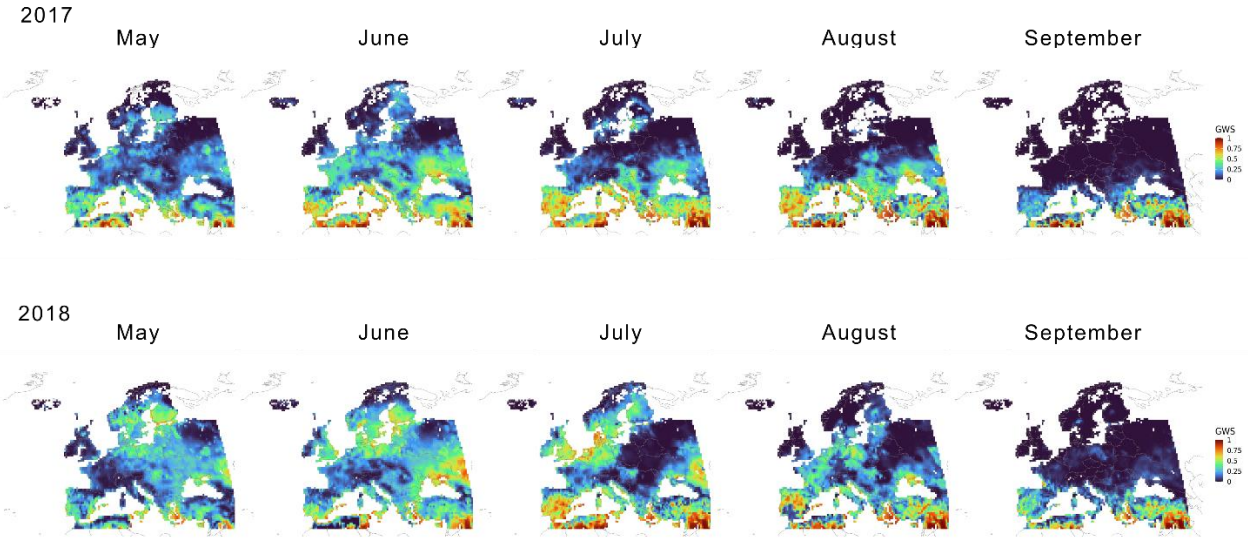

Figure S10: Comparison of GWS in the summer months in Europe in 2017 and 2018.

Blue water stress

Blue water stress is calculated for two scenarios, the no irrigation scenario INO and the limited irrigation scenario ILIM. Within ILIM, there are two options of calculation BWS: a) one classical approach only considering discharge as available water (as applied in the literature) *LIMq* and b) one approach considering not only discharge but also available water in reservoirs *ILIMq+r*.

BWS in this study only focuses on water availability within the gridcell considered. This gridcell can also withdraw irrigation water from neighboring upstream cells, but we do not account for these water flows from external grid cells in this study. Comparing the three approaches of calculating BWS shows that the INO scenario only includes a few cells that show moderate or high transgressions (stemming from transgressions in water use for industry and households) (ca. 28 Mha affected). *ILIMq* exhibits more transgressions (161 Mha affected), while BWS in *ILIMq+r* is mitigated by the water used from reservoirs to a small extent (153 Mha affected).

Table S2: Agricultural area affected by blue water stress in the INO and ILIM scenario (average for the time period 2015-2019). For ILIM, BWS was calculated considering discharge (ILIMq) as well as discharge and water in reservoirs as available water resources.

Agricultural area affected	INO	ILIMq	ILIMq+r
0 - 0.2	1528 Mha	1315 Mha	1329 Mha
0.2 - 0.4	25 Mha	109 Mha	125 Mha
0.4 - 1	26 Mha	155 Mha	125 Mha

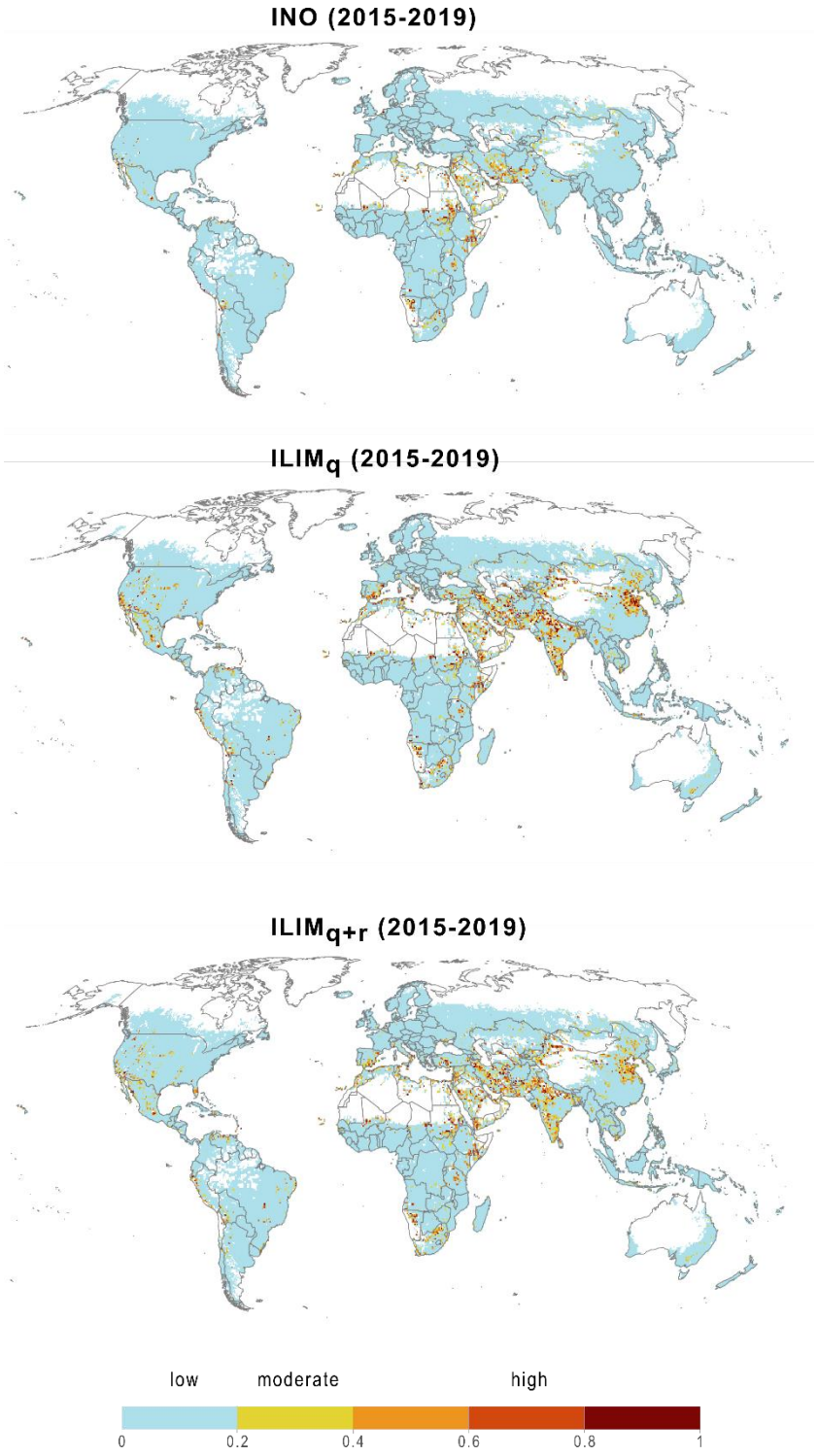

Figure S11: Blue water stress for INO, ILIMq and ILIMq+r (average over time period 2015-2019).

Combined water stresses

We analysed three combinations of water stresses, a) GWS and BWS of the INO scenario, b) GWS and BWS of the ILIM scenario where BWS was calculated only including discharge q, and c) GWS and BWS of the ILIM scenario where BWS was calculated including discharge q and water withdrawals from reservoirs r (see Fig. C7).

The main part of this study discusses the differences between a) and c), here we also include b) for comparisons. Figure C7 shows that differences between b) and c) are not very large. Only grid cells with reservoirs exhibit a lower BWS in c).

Figure C8 focuses on the shifts in water stresses only considering agricultural areas in cells with irrigation. Comparing b) and c) shows that when including reservoirs in c), areas that are not blue water stressed (BWS 0 - 0.2) increase, while moderately stressed areas increase by 2.3% and highly stressed areas decrease by 4.3%.

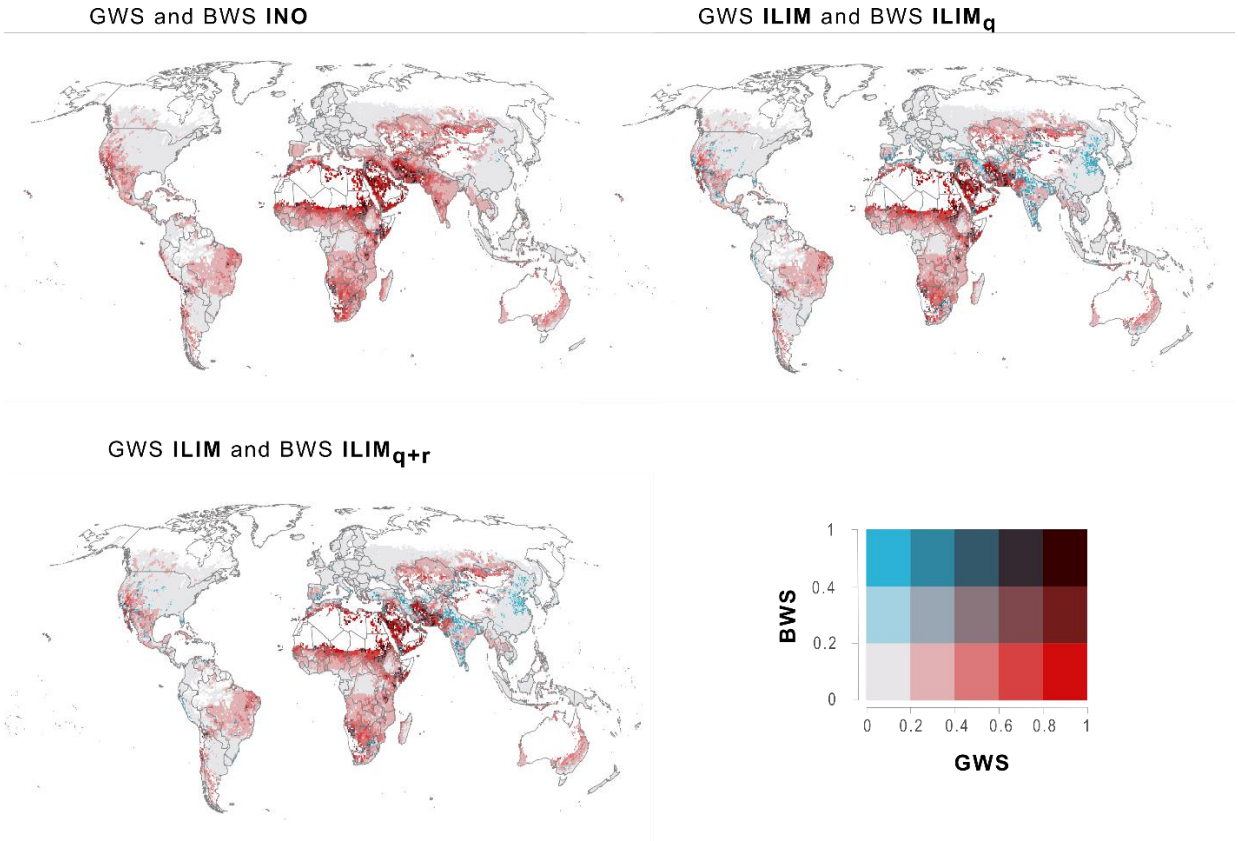

Figure S12: Combined water stresses: simulated spatial pattern of combined GWS and BWS under INO scenario, ILIM + ILIMq scenario and ILIM + ILIMq+r scenario (average over time period 2015-2019).

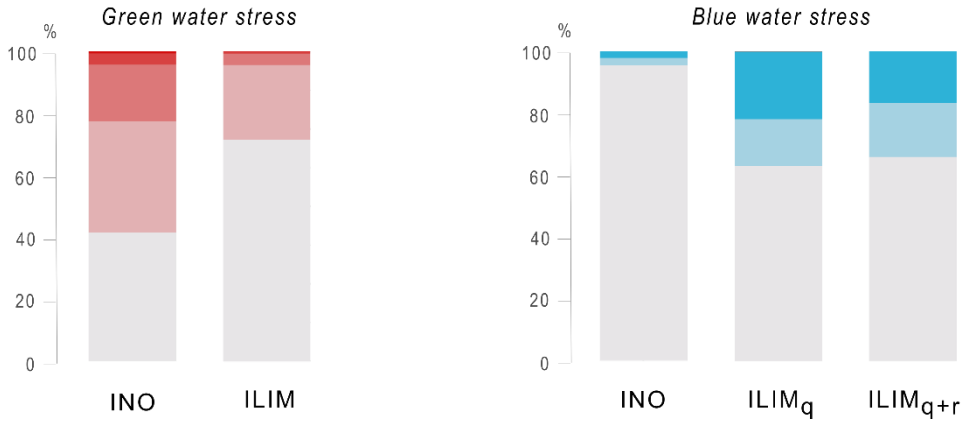

Figure S13: Shifts in water stresses: Here, only agricultural areas in cells with irrigation considered. Water stresses are simulated for GWS (INO and ILIM) and BWS (INO, ILIMq and ILIMq+r) and averaged over the time period 2015-2019.

Table S3: Agricultural area affected by GWS in cells with irrigation (average 2015-2019).

	INO	**ILIM**
0 - 0.2	286 Mha (41.5%)	492 Mha (71.5%)
0.2 - 0.4	247 Mha (35.9%)	167 Mha (24.2%)
0.4 - 0.6	126 Mha (18.3%)	26 Mha (3.7%)
0.6 - 0.8	25 Mha (3.7%)	4 Mha (0.6%)
0.8 - 1	5 Mha (0.7%)	3 Mha (0.04%)

Table S4: Agricultural area affected by BWS in cells with irrigation (average 2015-2019).

	INO	**ILIMq**	**ILIMq+r**
0 - 0.2	653 Mha (94.8%)	414 Mha (60.1%)	435 Mha (63.2%)
0.2 - 0.4	17 Mha (2.4%)	100 Mha (14.5%)	116 Mha (16.8%)
0.4 - 1	15 Mha (2.1%)	144 Mha (20.9%)	114 Mha (16.6%)

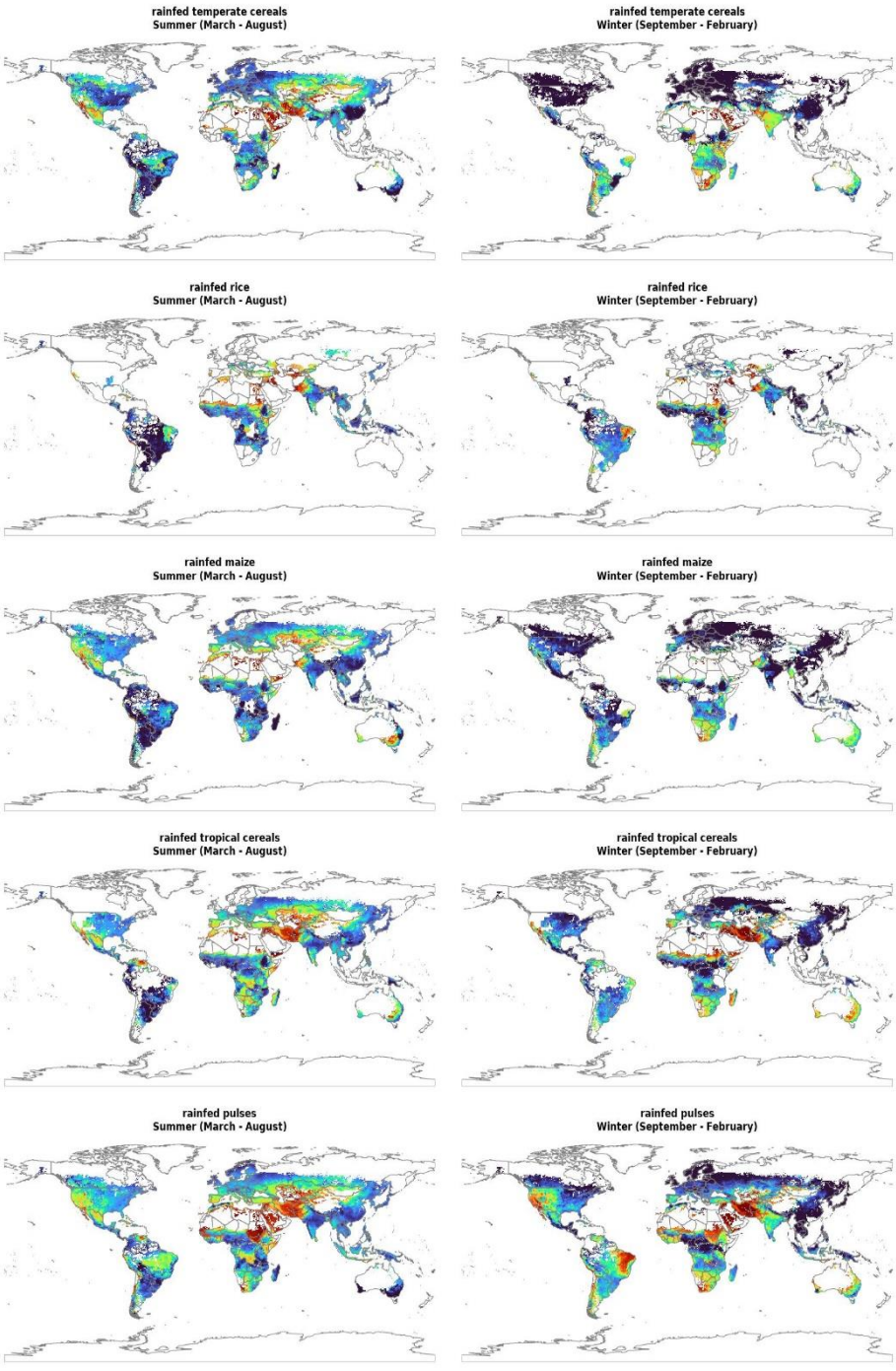
rainfed temperate cereals
Summer (March - August)
rainfed temperate cereals
Winter (September - February)
rainfed rice
Summer (March - August)
rainfed rice
Winter (September - February)
rainfed maize
Summer (March - August)
rainfed maize
Winter (September - February)
rainfed tropical cereals
Summer (March - August)
rainfed tropical cereals
Winter (September - February)
rainfed pulses
Summer (March - August)
rainfed pulses
Winter (September - February)

rainfed temperate roots
Summer (March - August)

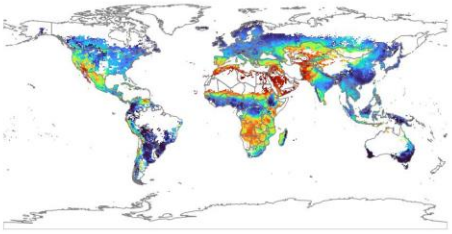

rainfed temperate roots
Winter (September - February)

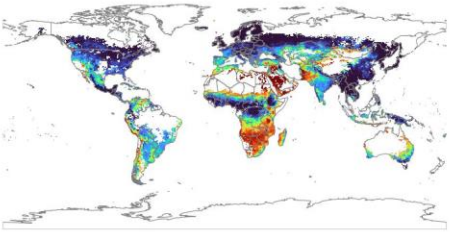

rainfed tropical roots
Summer (March - August)

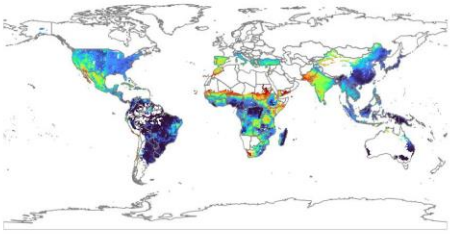

rainfed tropical roots
Winter (September - February)

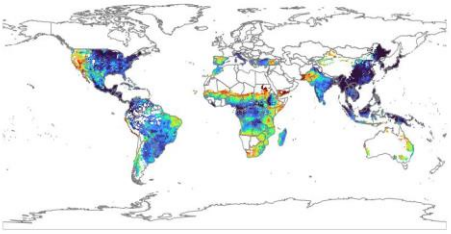

rainfed oil crops sunflower
Summer (March - August)

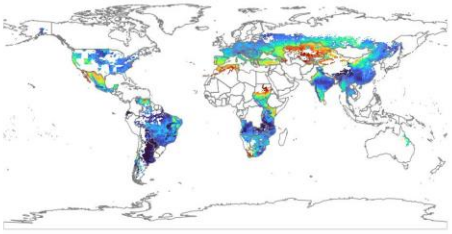

rainfed oil crops sunflower
Winter (September - February)

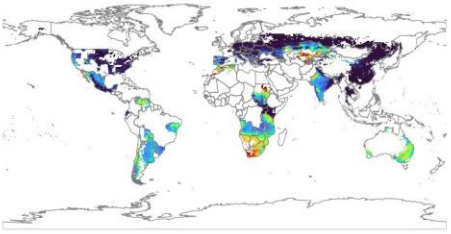

rainfed oil crops soybean
Summer (March - August)

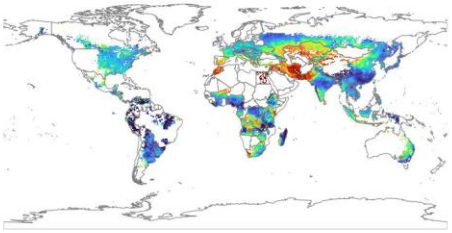

rainfed oil crops soybean
Winter (September - February)

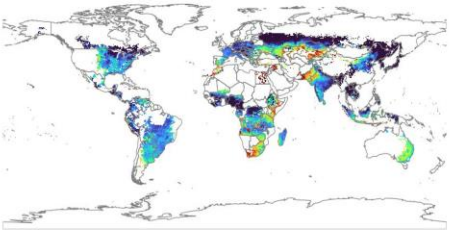

rainfed oil crops groundnut
Summer (March - August)

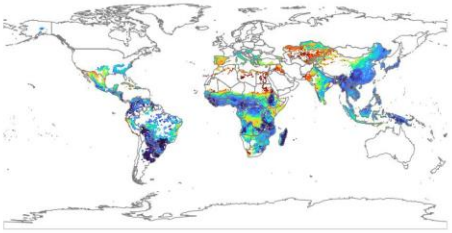

rainfed oil crops groundnut
Winter (September - February)

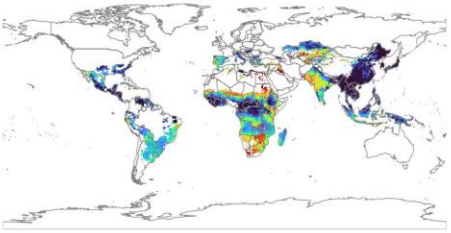

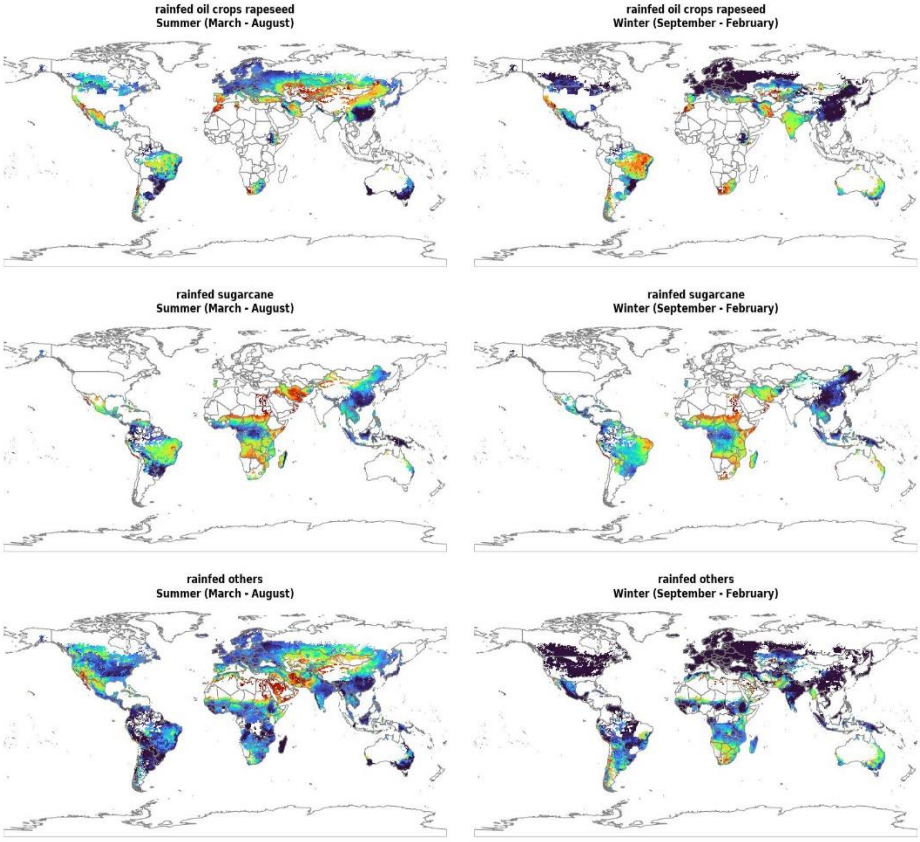

115

Figure S14: CFT-specific GWS of the rainfed CFTs in the ILIM scenario (averaged over the 2015-2019 for the summer and winter months).